Simultaneous intracellular chloride and pH measurements using a GFP-based sensor

Daniele Arosio[1,2], Fernanda Ricci[1,3,4], Laura Marchetti[1,4], Roberta Gualdani[1], Lorenzo Albertazzi[1,3] & Fabio Beltram[1,3]

Chloride and protons perform important closely related roles in many cellular responses. Here we developed a ratiometric biosensor, ClopHensor, based on a highly chloride-sensitive *Aequorea victoria* GFP variant that is suited for the combined real-time optical detection of pH changes and chloride fluxes in live cells. We detected high chloride concentration in large dense-core exocytosis granules by targeting ClopHensor to these intracellular compartments.

Chloride (Cl^-), the most abundant anion in living organisms, regulates many physiological processes including control of membrane potential, neurotransmission, regulation of cell volume and charge balance[1,2]. As a consequence, Cl^- homeostasis alterations lead to several human diseases[3]. Noninvasive monitoring of intracellular Cl^- concentration ($[Cl^-]_i$) is performed using fluorescent indicators, usually quinolinium-derived[4] indicators, which have been used for Cl^- transport studies in intact cells. The use of chemical dyes, however, is severely limited by their gradual leakage from labeled cells and need for excitation at ultraviolet wavelengths[2]. The observation that YFP fluorescence is quenched by halogens prompted the rapid development of $[Cl^-]_i$-monitoring methods based on YFP quenching[5]. The first ratiometric genetically encoded $[Cl^-]_i$ indicator, Clomeleon[6], was developed by linking YFP with the Cl^--insensitive CFP, a commonly used fluorescence resonance energy transfer (FRET) donor for YFP. Random[7] and rational[8] mutagenesis of YFP led to new indicators with improved Cl^- sensitivity, more suitable to monitor $[Cl^-]_i$ in the physiological range of 3–60 mM (ref. 2). Unfortunately, YFP-based indicators require independent means to assess pH values, as pH strongly influences YFP affinity for Cl^- (ref. 9); furthermore, the pH-sensitive CFP and YFP fluorescence complicates the interpretation of FRET signals[10] and the resulting quantification of $[Cl^-]_i$ (ref. 11). To overcome these difficulties, we developed a non–FRET-based sensor, ClopHensor, for measuring changes in $[Cl^-]_i$ and intracellular pH (pH_i) simultaneously.

We have previously shown that a highly specific anion-binding site can be engineered in enhanced GFP (EGFP) by the single substitution T203Y (E^2GFP)[12]. The new binding site has similar Cl^- affinity to that of the improved variants of Clomeleon[8] or YFP[7], although the binding site is in a different location in the protein[9,12]. ClopHensor exploits the spectral and chemical properties of the E^2GFP anion-binding site (**Fig. 1a** and **Supplementary Data**). We chose monomeric DsRed as a partner in the fusion construct because its fluorescence was insensitive to either Cl^- or H^+ and fairly separated from that of E^2GFP. Indeed, spectroscopic studies of the purified construct showed that fusion to DsRed has virtually no impact on the advantageous properties of E^2GFP. In particular, the pH isosbestic point[13] was the same in E^2GFP and ClopHensor excitation spectra (458 nm; **Fig. 1b**). Analysis at various pH and $[Cl^-]$ conditions also revealed biosensor spectral changes ideally suited for the ratiometric operation of the biosensor upon excitation at three wavelengths: 488-nm pH-dependent E^2GFP signal, 458-nm pH-independent E^2GFP signal, and 543-nm Cl^-- and pH-independent DsRed signal (**Fig. 1c**). Anion binding in E^2GFP is regulated by static quenching: a population of nonfluorescent protein is formed upon Cl^- binding so that no changes are displayed in the ratio between neutral and anionic E^2GFP excitation signals[13]. This property, which allows Cl^--independent ratiometric measurement of pH_i with E^2GFP[13], was also preserved in ClopHensor; thus the pH calibration curve could be derived from the ratio R_{pH} = green to cyan, free from the influence of $[Cl^-]_i$ (**Fig. 1d**,**e**). Conversely, ratiometric measurements of $[Cl^-]_i$ required pH-dependent calibration curves (**Fig. 1f**) derived from the ratio R_{Cl} = cyan to red. Crucially, Cl^- binding studies showed that H^+ and Cl^- bind the sensor in the same cooperative manner as has been reported for E^2GFP alone; thus, we applied the same scheme valid for E^2GFP (Online Methods, equation 4) to obtain Cl^- affinity of ClopHensor as a function of pH (**Supplementary Figs. 1** and **2**). In particular, we determined two setup-independent parameters (best fit ± s.d.) in solution at 37 °C: proton equilibrium of the Cl^- unligated form (acid dissociation constant, pK_a) = 6.81 ± 0.05 and Cl^- dissociation constant of the fully protonated form of the sensor ($^1K_d^{Cl}$)= 13.1 ± 0.5 mM.

Then we evaluated fluorescence response of ClopHensor in WSS-1 cells. We performed calibration at various pH_i and $[Cl^-]_i$ values by ionophore clamping technique. After excitation at 488, 458 and 543 nm (green, cyan and red channels, respectively), we sequentially acquired three-channel fluorescence images (**Fig. 2a**,**b**). We carefully chose fluorescence emission ranges to minimize spectral bleed-through; in particular, we selected the green- and cyan-channel emission ranges to reduce the

[1]National Enterprise for nanoScience and nanoTechnology, Istituto Nanoscienze, Consiglio Nazionale delle Ricerche and Scuola Normale Superiore, Pisa, Italy. [2]Istituto di Biofisica, Consiglio Nazionale delle Ricerche, Trento Povo, Italy. [3]Italian Institute of Technology at National Enterprise for nanoScience and nanoTechnology, Center for Nanotechnology Innovation, Pisa, Italy. [4]These authors equally contributed to this work. Correspondence should be addressed to D.A. (daniele.arosio@cnr.it).

RECEIVED 2 DECEMBER 2009; ACCEPTED 29 APRIL 2010; PUBLISHED ONLINE 27 JUNE 2010; DOI:10.1038/NMETH.1471

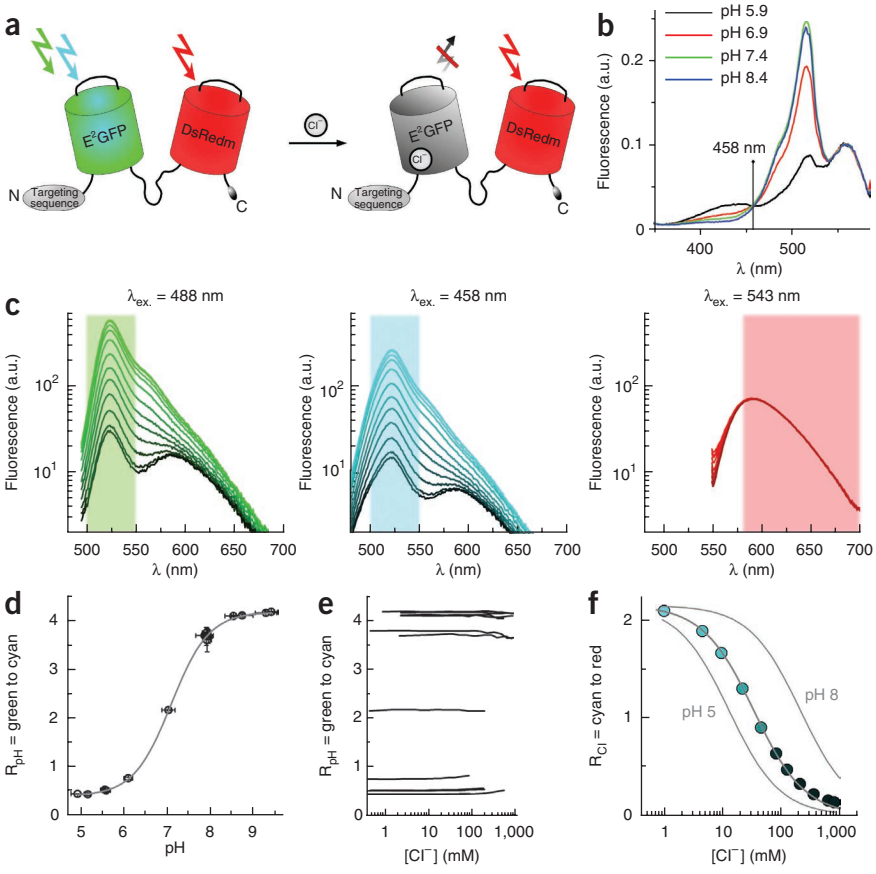

Figure 1 | ClopHensor design and functional characterization. (**a**) E^2GFP and DsRed monomer are fused by a flexible 20-amino-acid linker. Binding of Cl^- to E^2GFP induces static quenching of its fluorescence. (**b**) Excitation spectra of the purified construct at different pH values and emission set at 590 nm. An isosbestic point was present at about 458 nm. λ, wavelength. (**c**) Emission spectra of the purified ClopHensor construct after excitation at the indicated wavelengths ($\lambda_{ex.}$), collected at pH 6.9, 37 °C and $[Cl^-]$ from 0 (lightest-color line) to 1 M (darkest-color line). Shaded areas represent the collected emission ranges of the three channels used for the microscopy analysis in living cells. (**d**,**e**) Green-to-cyan ratio values of the purified construct at various pH and Cl^- values. Fitting curve in **e** was drawn using equation 6 in Online Methods. Error bars, s.d. for about 10 measurements collected at the various $[Cl^-]$ values reported in **e**. (**f**) Cyan-to-red ratio values computed from data in **c** (unlabeled curve). Fitting curve was drawn using equation 7 in Online Methods. Light to dark blue dots represent fluorescence quenching upon Cl^- binding.

cross-excitation cross-emission contribution of DsRed, and bleed-through artifacts were virtually absent in the red channel (**Fig. 1c**). We obtained pH_i and $[Cl^-]_i$ maps by calculating intensity ratios R_{pH} and R_{Cl}, respectively. Denominators of R_{pH} and R_{Cl} are respectively pH- and Cl^--independent signals allowing for straightforward data analysis (Online Methods). Additionally, in a typical experimental setup, such as the one used for this work, it was possible to record both green and cyan channels with the same photomultiplier voltage and emission range, so that evaluation of R_{pH} was influenced only by α, the ratio between excitation-beam intensities at 458 nm and 488 nm (**Fig. 2c**). Global fitting of αR_{pH}, from three sets of

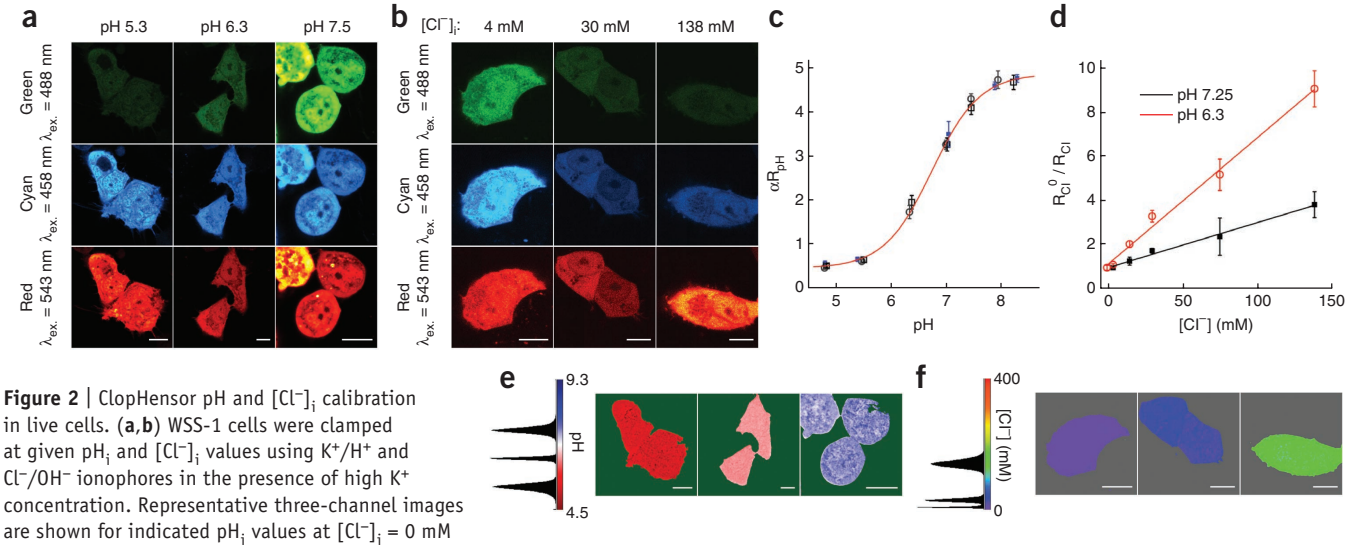

Figure 2 | ClopHensor pH and $[Cl^-]_i$ calibration in live cells. (**a**,**b**) WSS-1 cells were clamped at given pH_i and $[Cl^-]_i$ values using K^+/H^+ and Cl^-/OH^- ionophores in the presence of high K^+ concentration. Representative three-channel images are shown for indicated pH_i values at $[Cl^-]_i$ = 0 mM (**a**) and for indicated $[Cl^-]_i$ values at pH 6.3 (**b**). Scale bars, 5 µm. (**c**) Experimental green-to-cyan ratio (R_{pH}) as a function of pH_i, normalized by α, for three sets of cell cultures (different symbols). Data presented are means ± s.d. of ~20–30 cells. The pH calibration curve (red line) was calculated using equation 6 in Online Methods with best-fit parameters (± s.d.): $pK_a = 6.78 \pm 0.04$, with R_A and R_B denoting R values for the sensor in the acidic and basic form, respectively. $R_A = 0.469 \pm 0.014$ and $R_B = 4.948 \pm 0.04$. (**d**) Stern-Volmer plot of experimental cyan-to-red ratio (R_{Cl}). Data presented are means ± s.d. of 15 to 20 cells. K_d^{Cl} values of 17.1 and 49.2 mM calculated at pH 6.3 and 7.25, respectively (using equation 4 in Online Methods) were used to draw the calibration lines according to an adjusted form of equation 7 in Online Methods ($R_{Cl}^0/R_{Cl} = 1 + 1/K_d^{Cl}[Cl^-]$). (**e**,**f**) Representative pH_i and $[Cl^-]_i$ maps. Lookup tables display also the pixel-value distribution of pH_i (**e**) and $[Cl^-]_i$ (**f**) of the reported maps. Scale bars, 5 µm.

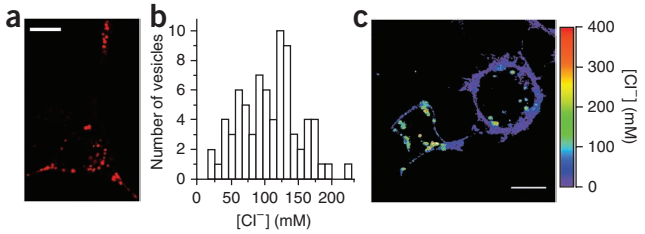

Figure 3 | Measurement of chloride concentration in LDCVs. (**a**) Micrograph of PC12 cells transfected with the NPY-ClopHensor plasmid that were differentiated by treatment with nerve growth factor (red channel). (**b**) Distribution of the measured LDCV $[Cl^-]_i$ in PC12 cells ($n = 76$). (**c**) $[Cl^-]_i$ map of WSS-1 cells co-expressing ClopHensor in LDCVs and at the plasma membrane. Scale bars, 5 µm.

cell cultures collected at different α values, provided the reference pH calibration we used here. The measurement of R_{Cl} (**Fig. 2d**) required two separate emission ranges for collecting E^2GFP and DsRed fluorescence signals, and the determination of a setup-dependent parameter (R^0_{Cl}) was necessary experiment by experiment. Yet we could easily estimate R^0_{Cl} by the cyan-to-red ratio, independently from pH, in cells clamped at $[Cl^-]_i$ of 0 mM. ClopHensor characteristics determined the following operational order: (i) estimate pH_i in a region of interest; (ii) calculate the corresponding K_d^{Cl} (pH); (iii) use this value to estimate $[Cl^-]_i$ in the selected region of interest. Using this procedure, we measured pH_i and $[Cl^-]_i$ maps simultaneously in WSS-1 cells and obtained average (mean ± s.d.; $n = 150$) pH_i of 7.3 ± 0.2 and $[Cl^-]_i$ of 19 ± 14 mM, in agreement with values reported for many cell types[2,13,14]. The relatively large uncertainty for $[Cl^-]_i$ was due to a substantial cell-to-cell variation under physiological conditions, and we did not observe this in the presence of ionophores that not only equilibrated $[Cl^-]_i$ throughout the cell but also appeared to reduce cell-to-cell $[Cl^-]_i$ variation (**Fig. 2e**,**f**). Furthermore, we examined the capability of ClopHensor to report real-time dynamic changes of $[Cl^-]_i$ (**Supplementary Figs. 3–5** and **Supplementary Table 1**).

The interior of large dense-core vesicles (LDCVs), the dominant secretory organelles in neuroendocrine cells, has so far eluded quantification of $[Cl^-]_i$ mostly because of the inner acidic environment (pH = 5.4) that quenches an indicator's fluorescence[1], for example, YFP. To test whether ClopHensor allows quantification of LDCV $[Cl^-]_i$, we fused it to the N-terminal signal sequence of neuropeptide Y (NPY), which is known to target green fluorescent proteins into LDCVs[15]. In PC12 cells, NPY-ClopHensor displayed bright fluorescence spots, which accumulated in neurites, as expected (**Fig. 3a**). ClopHensor allowed us to measure the average LDCV pH_i of 5.2 ± 0.4 (mean ± s.d.; $n = 76$) in agreement with reported findings[1] and to reveal, to our knowledge for the first time, high Cl^- concentration inside an LDCV. The average LDCV $[Cl^-]_i$ was 110 mM but with large variability (s.d., 48 mM) (**Fig. 3b**). This variability may reflect dynamic changes of LDCV $[Cl^-]_i$ during exocytosis processes that deserve further studies. Because these conditions pushed ClopHensor to its operational limit (**Supplementary Fig. 6**), we fused it to a sequence containing two palmitoylation sites and targeted the resulting sensor, PalmPalm-ClopHensor, to the plasma membrane to allow direct comparison of the high LDCV $[Cl^-]_i$ with the lower $[Cl^-]_i$ values simultaneously measured at the plasma membrane (**Fig. 3c**). The $[Cl^-]_i$ distribution peaked at about 130 mM in LDCV regions and 20 mM in plasma-membrane regions, in agreement with the value measured in the whole cytoplasm (19 mM). Similarly to PC12 cells, in WSS-1 cells, the average values (mean ± s.d., $n = 150$) measured in LDCVs were $pH_i = 5.6 \pm 0.5$ and $[Cl^-]_i = 122 \pm 40$ mM. Acidification is required by secretory granules maturation after sorting in the *trans*-Golgi network, where $[Cl^-]_G$ is 50 mM and pH_G is 6.4 (ref. 14). Our data revealed that a substantial Cl^- accumulation correlated with acidification in LDCV, confirming that Cl^- is the main counterion used by living systems to balance H^+ accumulation[1].

Our results show that ClopHensor is a powerful and flexible tool to visualize Cl^- and H^+ fluxes. The spatial and temporal resolution attained in this study indicates the efficacy of ClopHensor in monitoring biological processes in which Cl^- and H^+ have a combined role.

METHODS

Methods and any associated references are available in the online version of the paper at http://www.nature.com/naturemethods/.

Note: Supplementary information is available on the Nature Methods website.

ACKNOWLEDGMENTS

We thank P. Faraci for his assistance in preparing NPY-ClopHensor PC12 cell samples, S. Luin for his assistance with microscope analysis, S. Sulis-Sato and G. Lanza for their help with experimental setup, A. Cereseto for critical reading of the manuscript and G. Ratto for helpful discussions. The study was supported by *Fondazione Monte dei Paschi di Siena* (Monte dei Paschi Foundation) and by the Italian Ministry for University and Research (Fondo per gli Investimenti della Ricerca di Base RBLA03ER38).

AUTHOR CONTRIBUTIONS

D.A. conceived the sensor, designed and performed experiments, analyzed data and wrote the paper; F.R. and L.M. generated ClopHensor constructs, and designed and performed experiments; R.G. performed sensor calibrations and kinetic analysis; L.A. performed experiments and analyzed data; F.B. interpreted the data, edited the paper and gave conceptual advice.

COMPETING FINANCIAL INTERESTS

The authors declare no competing financial interests.

Published online at http://www.nature.com/naturemethods/.
Reprints and permissions information is available online at http://npg.nature.com/reprintsandpermissions/.

1. Faundez, V. & Hartzell, H.C. *Sci. STKE* **2004**, re8 (2004).
2. Bregestovski, P., Waseem, T. & Mukhtarov, M. *Front. Mol. Neurosci.* **2**, 15 (2009).
3. Planells-Cases, R. & Jentsch, T.J. *Biochim Biophys Acta* **1792**, 173–189 (2009).
4. Illsley, N.P. & Verkman, A.S. *Biochemistry* **26**, 1215–1219 (1987).
5. Jayaraman, S., Haggie, P., Wachter, R.M., Remington, S.J. & Verkman, A.S. *J. Biol. Chem.* **275**, 6047–6050 (2000).
6. Kuner, T. & Augustine, G.J. *Neuron* **27**, 447–459 (2000).
7. Galietta, L.J., Haggie, P.M. & Verkman, A.S. *FEBS Lett.* **499**, 220–224 (2001).
8. Markova, O., Mukhtarov, M., Real, E., Jacob, Y. & Bregestovski, P. *J. Neurosci. Methods* **170**, 67–76 (2008).
9. Wachter, R.M., Yarbrough, D., Kallio, K. & Remington, S.J. *J. Mol. Biol.* **301**, 157–171 (2000).
10. Tsutsui, H., Karasawa, S., Okamura, Y. & Miyawaki, A. *Nat. Methods* **5**, 683–685 (2008).
11. Jose, M., Nair, D.K., Reissner, C., Hartig, R. & Zuschratter, W. *Biophys. J.* **92**, 2237–2254 (2007).
12. Arosio, D. *et al. Biophys. J.* **93**, 232–244 (2007).
13. Bizzarri, R. *et al. Biophys. J.* **90**, 3300–3314 (2006).
14. Wu, M.M. *et al. Chem. Biol.* **7**, 197–209 (2000).
15. El Meskini, R. *et al. Endocrinology* **142**, 864–873 (2001).

ONLINE METHODS

Ratio imaging pH_i and $[Cl^-]_i$ maps. Spectroscopic dual-wavelength for the numerator (s_N) and denominator (s_D) of ratiometric

$$(R \equiv s_N / s_D)$$

measurements with the formation of a 1:1 (analyte:sensor) complex lead to an equilibrium described by the Grynkiewicz equation[16], which for a general $[Cl^-]$ indicator can be written as follows:

$$[Cl^-] = K_d^{Cl}\left(\frac{R - R_{free}}{R_{bound} - R}\right)\left(\frac{s_{D,free}}{s_{D,bound}}\right) \quad (1)$$

In equation 1, K_d^{Cl} is the chloride dissociation constant, R_{free} is the R plateau value for the Cl^--free indicator, R_{bound} is the plateau for the Cl^--bound indicator, $s_{D,free}$ and $s_{N,bound}$ are the signals, at the denominator of R, originating from the unbound and Cl^--bound indicator, respectively.

Likewise, the Grynkiewicz equation for a general pH indicator can be written as:

$$pH = pK_a + \log\left(\frac{R - R_A}{R_B - R}\right) + \log\left(\frac{s_{D,A}}{s_{D,B}}\right) \quad (2)$$

In equation 2, R_A and R_B are the values of R for the indicator in the acidic and basic form, respectively; and $s_{D,A}$ and $s_{D,B}$ are the values of s_D for the indicator in the acidic and basic form, respectively. In contrast to the dissociation constant used in equation 1, pK_a is the logarithm of an association constant (see also ref. 17).

In the case of ClopHensor, the cyan fluorescence is pH independent (458-nm isosbestic excitation), so that $s_{D,B} = s_{D,A}$ and pH_i maps were computed according to the following equation:

$$pH_i = pK_a + \log\left(\frac{\alpha R_{pH} - R_A}{R_B - \alpha R_{pH}}\right) \quad (3)$$

in which $pK_a = 6.78$, $R_A = 0.469$, $R_B = 4.948$, R_{pH} is green-to-cyan ratio and α is the ratio between excitation-beam intensities at 458 nm and 488 nm ($I_{458\,nm}/I_{488\,nm}$), the recorded ratio of excitation intensities. To update laser-intensity fluctuations dynamically, we used the microscope transmission optical system following the alignment procedures previously described[18,19].

Once a region-of-interest pH_i value was estimated, the corresponding K_d^{Cl} value was calculated according to equation (4) (see reference 12 equations 4 and 6) with $pK_a = 6.81$ and ${}^1K_d^{Cl} = 13.1$ mM.

$$K_d^{Cl}(pH) = {}^1K_d^{Cl}\frac{1 + 10^{(pK_a - pH)}}{10^{(pK_a - pH)}} \quad (4)$$

Additionally, in consideration of the fact that $s_{D,free} = s_{D,bound}$ because the red channel (DsRed) fluorescence is Cl^- independent and $R_{bound} = 0$ because of the E^2GFP fluorescence static quenching, equation 1 can be simplified to equation 5, so that $[Cl^-]_i$ maps were calculated according to:

$$[Cl^-]_i = K_d^{Cl}(pH)\frac{R_{Cl}^0 - \alpha_2 R_{Cl}}{\alpha_2 R_{Cl}} \quad (5)$$

Where R_{Cl} is cyan-to-red ratio, $\alpha_2 = I_{543\,nm}/I_{458\,nm}$, the recorded ratio of excitation intensities and R_{Cl}^0, a setup-dependent parameter, was determined experiment by experiment from a single measurement at $[Cl^-]_i = 0$ and any pH value from 6.0 to 7.8; in fact, the cyan channel was pH independent. R_{Cl}^0 varied from 1 to 5 in our experimental conditions.

Accordingly, calibration data were fitted rewriting equations 3 and 5 as in equations 6 and 7, respectively.

$$\alpha R_{pH} = \frac{R_B + R_A 10^{(pK_a - pH)}}{1 + 10^{(pK_a - pH)}} \quad (6)$$

$$\alpha_2 R_{Cl} = \frac{R_{Cl}^0}{1 + [Cl^-]/K_d^{Cl}} \quad (7)$$

Gene construction. The *E^2GFP-DsRedm* bacterial expression plasmid was prepared according to the following procedure. Sequence encoding E^2GFP was PCR-amplified from the pPR-IBA2-E^2GFP plasmid[12] using primers BsaI-E^2-fw and E^2-BamHI-rv (**Supplementary Table 2**). Sequence encoding the amino acid linker RGSASGGGGGLVPRGSASGA fused to dsRed was obtained by two sequential PCRs on pDsRed-Monomer vector (Clontech) using the forward primer DsRed-fw or BamHI-linker-fw and the reverse primer DsRed-BsaI-rv. The two inserts were digested with BsaI and BamHI, and then cloned into the pPR-IBA2 vector (IBA) with triple ligation.

For expression in mammalian cells, the *E^2GFP* insert was obtained by PCR amplification using primers HindIII-E^2-fw and E^2-BamHI-rv and subcloned into the pcDNA3.1(+) vector (Invitrogen) using HindIII and BamHI. The *linker-DsRedm* insert was obtained as described above but using the DsRed-XbaI-rv reverse primer and BamHI and XbaI restriction sites. All PCR primers were purchased from Sigma-Genosys and all restriction endonucleases from New England Biolabs. *Gap43* (ref. 20) and *NPY*[15] sequences were inserted at the 5′ end of the biosensor sequence by annealing the primers Gap20-fw and NPY-fw, respectively, with their complementary sequences (**Supplementary Table 2**). All the constructs were verified by sequencing the entire insert (**Supplementary Data**).

Expression and purification of ClopHensor *in vitro*. Recombinant ClopHensor was expressed as strep-tagged protein[12] in *Escherichia coli* BL21 (DE3) strain (Invitrogen) and collected 20 h after induction with IPTG at 30 °C. Purification by affinity was carried out using strepTactin Superflow 5-ml cartridges (IBA) following manufacturer's instructions, at 4 °C in an AKTA Basic10 FPLC system (GE Healthcare) with continuous monitoring of optical densities at 280, 410 and 560 nm. The use of chloride-free buffers in a final purification step ensured the complete removal of Cl^- from preparations; anion exchange was performed with ResourceQ 6-ml cartridge (GE Healthcare) using a linear gradient (10 column volumes duration) from 0 to 250 mM Na_2SO_4 in 20 mM diethanolamine (pH 8.5).

Fluorometry. Fluorescence measurements and analysis were carried out as previously detailed[12] using a Cary Eclipse fluorometer (Varian). Typically, 1.92-ml samples were used in a quartz cuvette (Hellma) at 37 ± 0.1 °C or 20 ± 0.1 °C for comparison between the fusion construct and the single protein. All binding curves were fitted with a simple 1:1 binding equation using Origin 7.0 (OriginLab). Kinetic measurements of the recombinant ClopHensor were done in the same fluorescence spectrometer equipped with the rapid-mixing stopped-flow unit RX 2000 (Applied Photophysics). Fluorescence traces were measured with the integration time of 12.5 ms in response to rapid changes in

solution [Cl^-] (from 0 to a value in the range of 4–138 mM). Excitation wavelength was 510 ± 10 nm and emission 523 ± 5 nm; for the pH 5.0 data excitation was set at 435 ± 5 nm and emission at 508 ± 5 nm. Temperature was controlled at 37 °C, and protein concentration was 0.7 μM.

Cell culture and transfection. Human embryonic kidney 293 cells, stably expressing gamma-aminobutyric acid A ($GABA_A$) receptor, were from American Type Culture Collection (WSS-1 cells[21]). Cells were grown in Dulbecco's modified Eagle's medium (Gibco), supplemented with 2 mM L-glutamine, 1 mM sodium pyruvate, 10% FBS (Gibco) and 10 μg l^{-1} penicillin-streptomycin. Subconfluent cells were plated in polylysine (Sigma)-coated 35-mm diameter coverglasses (WillCo-dish) and transfected using Effectene reagent (Qiagen) following the manufacturer's protocol. Cells were maintained in a 5% CO_2 atmosphere at 37 °C and imaged 2–3 d after transfection.

Calibration *in vivo*. The desired $[Cl^-]_i$ and pH_i were controlled by equilibrating extra- and intracellular ion concentrations using the K^+/H^+ exchanger nigericin (5 μM), the protonophore carbonyl cyanide p-chlorophenylhydrazone (CCCP) (5 μM), the K^+ ionophore valinomycin (5 μM) and the Cl^-/OH^- exchanger tributyltinchloride (10 μM) in the presence of high-K^+ 20 mM Hepes buffer containing 0.6 mM $MgSO_4$, 38 mM sodium gluconate and 100 mM potassium gluconate. Specified amount of gluconate anion was replaced by Cl^-, and pH was adjusted with small aliquots of NaOH. To avoid CO_2-dependent pH shift during calibrations, cells were maintained in CO_2-free atmosphere at 37 °C. Medium was replaced with proper buffer and changed four times to ensure stabilization of intracellular ionic concentrations.

Fluorescence multichannel images (n = 15–30 independent images, 3–5 acquisitions) were collected for each condition (pH and $[Cl^-]_i$ values). Green-to-cyan and cyan-to-red ratios were expressed as mean ± s.d.

Fluorescence imaging and analysis. Fluorescence images were collected using a Leica laser-scanning confocal inverted microscope TCS SP2 AOBS equipped with an HCX PL APO oil-immersion objective (40× magnification, 1.25 numerical aperture) and a CO_2 and temperature controller (CTI 3700). Excitation of E^2GFP at 458 nm and 488 nm was provided by an argon laser, and excitation of DsRed monomer was provided by either a He-Ne laser at 543 nm or a solid-state laser at 561 nm (DPSS 561, Melles Griot). A power meter (Newport, 841-PE with detector 818-ST-UV) was used to measure the laser beam power at the objective entrance. Typical measured power was 60 μW, 20 μW and 50 μW ± 40% (mean ± s.d.) for laser lines at 458 nm, 488 nm and 543 nm (or 561 nm), respectively. To minimize bleed-through artifacts, channel emissions were chosen as follows. Green channel fluorescence $(F)_{488\,nm}$ (488 nm excitation) was detected from 500 nm to 550 nm; cyan channel $F_{458\,nm}$ (458 nm excitation) was detected from 500 nm to 550 nm; and red channel $F_{543\,nm}$ (543 nm excitation) was detected from 580 nm to 700 nm. PMT voltage was kept constant at 550 nm. Laser scanning was performed using 400 Hz line frequency, 512 × 512 pixel format and pinhole aperture set at 1 airy disk unless otherwise stated. For instance, ClopHensor localization into LDCVs generated dimmer signals and required increasing excitation intensities (3 times as much) and confocal pinhole aperture (2.5 airy).

Image processing was performed using custom ImageJ (US National Institutes of Health) macros that could be applied to sets of images in a consistent and unbiased way. Mean background fluorescence measured either in nontransfected cells or in empty spaces indicated absence of autofluorescence; background owing to dark current and ambient light was subtracted before computing pixel-by-pixel division of images.

Images were semi-automatically segmented on the basis of pixel intensity with isodata algorithm ('getAutoThreshold' method or 'make binary' function in ImageJ) and binary masks (that is, 0 for background and 1 for cell objects) created. Multiplying each channel with the binary mask, we obtained masked images, which only contain values (above 0) for cellular regions. This procedure easily discriminated the regions of interest and prevented artifacts arising from dividing background-by-background values.

16. Grynkiewicz, G., Poenie, M. & Tsien, R.Y. *J. Biol. Chem.* **260**, 3440–3450 (1985).
17. Valeur, B. *Molecular Fluorescence: Principles and Applications* (Wiley-VCH, 2002).
18. Zucker, R.M. & Price, O. *Cytometry* **44**, 273–294 (2001).
19. Zucker, R.M. & Price, O.T. *Cytometry* **44**, 295–308 (2001).
20. Zacharias, D.A., Violin, J.D., Newton, A.C. & Tsien, R.Y. *Science* **296**, 913–916 (2002).
21. Wong, G., Sei, Y. & Skolnick, P. *Mol. Pharmacol.* **42**, 996–1003 (1992).

doi:10.1038/nmeth.1471